

Majorana edge modes in the Kitaev model

Manisha Thakurathi¹, K. Sengupta², and Diptiman Sen¹

¹Centre for High Energy Physics, Indian Institute of Science, Bangalore 560 012, India

²Theoretical Physics Department, Indian Association for the Cultivation of Science, Jadavpur, Kolkata 700 032, India

(Dated: June 3, 2014)

We study the Majorana modes, both equilibrium and Floquet, which can appear at the edges of the Kitaev model on the honeycomb lattice. We first present the analytical solutions known for the equilibrium Majorana edge modes for both zigzag and armchair edges of a semi-infinite Kitaev model and chart the parameter regimes of the model in which they appear. We then examine how edge modes can be generated if the Kitaev coupling on the bonds perpendicular to the edge is varied periodically in time as periodic δ -function kicks. We derive a general condition for the appearance and disappearance of the Floquet edge modes as a function of the drive frequency for a generic d -dimensional integrable system. We confirm this general condition for the Kitaev model with a finite width by mapping it to a one-dimensional model. Our numerical and analytical study of this problem shows that Floquet Majorana modes can appear on some edges in the kicked system even when the corresponding equilibrium Hamiltonian has no Majorana mode solutions on those edges. We support our analytical studies by numerics for finite sized system which show that periodic kicks can generate modes at the edges and the corners of the lattice.

PACS numbers: 75.10.Jm, 71.10.Pm, 03.65.Vf

I. INTRODUCTION

There have been extensive theoretical and experimental studies of topological phases of matter in recent years^{1–3}. Systems in these phases exhibit a bulk-boundary correspondence, namely, non-trivial topological properties of the gapped states in the bulk are related to gapless states at the boundary. The number of species of gapless boundary modes is typically determined by bulk topological invariant(s) whose nature depends on the spatial dimensionality of the system and its symmetries. Examples of systems with topological phases include two- and three-dimensional (2D and 3D) topological insulators, quantum Hall systems, 1D semiconducting wires with strong spin-orbit coupling and induced superconductivity, and unconventional superconductors.

The Kitaev model on a honeycomb lattice and the Kitaev chain (which is one of the models used to describe a wire with p -wave superconductivity) provide well-known examples of systems with such a bulk-boundary correspondence^{4–8}. The physics of the bulk of these systems has a natural description in terms of Majorana fermions. In addition, the edge physics of the Kitaev chain and its several variants have been studied in great detail. It is well-known that a finite length chain has Majorana modes at its two ends^{9–45}. A number of experimental realizations of such models have found evidence for such Majorana modes^{46–50}. However, the edge states of the Kitaev honeycomb model has not been studied in as much detail. Some discussion appears in Refs. [4,8] in the context of such states; however the analysis of Ref. 8 does not address the geometry of the edge and the full parameter range of the model. There has also been some discussion of localized Majorana modes in the bulk of this model in the presence of dislocations⁵¹.

Recently, there have been several studies of systems

in which the Hamiltonian varies with time in a periodic way which gives rise to edge or boundary states^{52–78}. Photonic systems with edge states have been demonstrated experimentally⁷⁹. Some of the theoretical papers have studied the boundary modes (called Floquet modes) in these systems and the associated topological invariants^{52–54,59,66–69,71,77}. In particular, Refs. [54,67,77] have discussed Floquet modes of the Majorana type at the ends of one-dimensional (1D) systems like the Kitaev chain. Floquet edge modes of the Kitaev honeycomb model have, however, not been studied so far to the best of our knowledge.

In this paper, we study the edge modes of the Kitaev honeycomb model for both a time-independent Hamiltonian and for a periodic driving of one of the parameters in the Hamiltonian. We consider a semi-infinite Kitaev model and review the known analytical solutions for the edge problem for both the zigzag and the armchair edges of the model. The existence of edge states are known to depend both on the type of edge (armchair or zigzag) and on the values of the coupling parameters of the model leading to an phase diagram showing the presence/absence of these states. For any set of values of the coupling parameters of the model, there exists a range of values of the transverse momentum k for which the edge states exist. We show that the edge modes have zero energy and the associated operators are of the Majorana type, corresponding to equal superpositions of $\pm k$ states. We also discuss the properties of these edge states which distinguishes them from their bulk counterparts. Our equilibrium analysis is followed by a discussion of the formalism for studying generation of non-equilibrium Floquet edge states in the presence of a periodic δ -function kick which changes the Kitaev coupling on the bonds perpendicular to the edge. We provide a concrete numerical method for the detection of such Floquet edge modes

via computation of the inverse participation ratio of the eigenstates of the Floquet Hamiltonian. We also develop an analytical understanding for the appearance and disappearance of these Floquet edge modes as a function of the drive frequency by providing a general formula for the momentum-dependent drive frequency at which such phenomenon occurs for an arbitrary d -dimensional integrable model. We show that the δ -function kicks can generate modes on certain edges even in the parameter regime where the time-independent Kitaev Hamiltonian has no edge solution. For a system with infinitely long edges but finite width, the problem can be mapped to a finite system in one dimension running in the direction transverse to the edges; the parameters of this 1D system depend on the couplings, the drive frequency and the transverse momentum k . This reduction to one dimension enables us to use some results from Ref. 77 regarding the Floquet Majorana modes. For a system which is finite in both directions, we study the problem numerically and demonstrate the existence of a variety of Floquet modes; some of these modes lie on the edges while the others lie only at the corners of the system.

The plan of the rest of this paper is as follows. In Sec. II, we review some of the properties of the Kitaev honeycomb model, its energy-momentum dispersion in the bulk, and the phase diagram. This is followed by Sec. III, where we study the edge modes in equilibrium. In Sec. IV, we provide a discussion of the formalism for detection of the Floquet edge modes. This is followed by Sec. V where we apply this formalism to the Kitaev model with periodic δ -function kicks. We show how the problem can be mapped to a one-dimensional system thus enabling us to analytically find the driving frequencies where edge modes appear or disappear. Finally, we conclude in Sec. VI.

II. KITAEV HONEYCOMB MODEL

The Kitaev model consists of spin-1/2's placed on the sites of a honeycomb lattice with a Hamiltonian of the form

$$H = \sum_{j+l=\text{even}} (J_1 \sigma_{j,l}^x \sigma_{j+1,l}^x + J_2 \sigma_{j-1,l}^y \sigma_{j,l}^y + J_3 \sigma_{j,l}^z \sigma_{j,l+1}^z), \quad (1)$$

where j, l are the column and row indices respectively, $\sigma_{m,n}^a$ are Pauli matrices at the site labeled (m, n) , and J_1 , J_2 and J_3 are the coupling parameters. In this section we will assume that all the couplings are time-independent. Let us also assume that all the $J_i \geq 0$.

A picture of the honeycomb lattice is shown in Fig. 1. We take the unit cells of the lattice to be the vertical bonds with sites labeled A and B ; these have $j + l$ equal to odd and even integers respectively. If the number of sites is denoted by N (assumed to be even), the number of unit cells is $N/2$. It is convenient to set the nearest-neighbor distance to be $1/\sqrt{3}$. Each unit cell is then

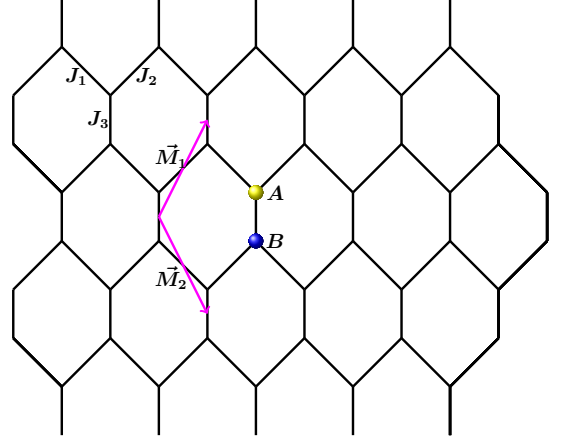


FIG. 1: (Color online) Kitaev model on the honeycomb lattice with xx coupling J_1 , yy coupling J_2 and zz coupling J_3 . \vec{M}_1 and \vec{M}_2 are the spanning vectors of the lattice, and A and B denote the two sites of a unit cell.

labeled by a vector $\vec{n} = \hat{i}n_1 + (\frac{1}{2}\hat{i} + \frac{\sqrt{3}}{2}\hat{j})n_2$, where n_1 , n_2 are integers which are related to the coordinates of the B site in that unit cell as $n_1 = (j - l)/2$ and $n_2 = l$. Fig. 1 shows the spanning vectors $\vec{M}_1 = \frac{1}{2}\hat{i} + \frac{\sqrt{3}}{2}\hat{j}$ and $\vec{M}_2 = \frac{1}{2}\hat{i} - \frac{\sqrt{3}}{2}\hat{j}$ which join some neighboring unit cells.

We now introduce the Majorana operators^{4,5}

$$\begin{aligned} \hat{a}_{j,l} &= \left(\prod_{i=-\infty}^{j-1} \sigma_{i,l}^z \right) \sigma_{j,l}^y, \quad \text{for } j + l = \text{even} \\ \hat{b}_{j,l} &= \left(\prod_{i=-\infty}^{j-1} \sigma_{i,l}^z \right) \sigma_{j,l}^x, \quad \text{for } j + l = \text{odd}. \end{aligned} \quad (2)$$

These are Hermitian operators satisfying the anti-commutation relations $\{\hat{a}_{m,n}, \hat{a}_{m',n'}\} = 2\delta_{mm'}\delta_{nn'}$, $\{\hat{b}_{m,n}, \hat{b}_{m',n'}\} = 2\delta_{mm'}\delta_{nn'}$, and $\{\hat{a}_{m,n}, \hat{b}_{m',n'}\} = 0$. In terms of these operators the Hamiltonian takes the form

$$H = i \sum_{\vec{n}} (J_1 \hat{b}_{\vec{n}} \hat{a}_{\vec{n}-\vec{M}_1} + J_2 \hat{b}_{\vec{n}} \hat{a}_{\vec{n}-\vec{M}_1} + J_3 \hat{D}_{\vec{n}} \hat{b}_{\vec{n}} \hat{a}_{\vec{n}}). \quad (3)$$

The $\hat{D}_{\vec{n}}$'s are operators which commute with each other and with the Hamiltonian; their eigenvalues can take the values ± 1 independently for each \vec{n} , thereby decomposing the 2^N -dimensional Hilbert space into $2^{N/2}$ sectors. It is known that the ground state of the model lies in the sector in which $\hat{D}_{\vec{n}} = 1$ for all \vec{n} ; we will work in this sector throughout this paper.

The Fourier transforms of the Majorana operators are defined as

$$\begin{aligned} \hat{a}_{\vec{n}} &= \sqrt{\frac{4}{N}} \sum_{\vec{k} \in \frac{1}{2}\text{BZ}} (\hat{a}_{\vec{k}} e^{i\vec{k} \cdot \vec{n}} + \hat{a}_{\vec{k}}^\dagger e^{-i\vec{k} \cdot \vec{n}}), \\ \hat{b}_{\vec{n}} &= \sqrt{\frac{4}{N}} \sum_{\vec{k} \in \frac{1}{2}\text{BZ}} (\hat{b}_{\vec{k}} e^{i\vec{k} \cdot \vec{n}} + \hat{b}_{\vec{k}}^\dagger e^{-i\vec{k} \cdot \vec{n}}), \end{aligned} \quad (4)$$

which satisfy the anticommutation relations $\{\hat{a}_{\vec{k}}, \hat{a}_{\vec{k}'}^\dagger\} = \{\hat{b}_{\vec{k}}, \hat{b}_{\vec{k}'}^\dagger\} = \delta_{\vec{k}, \vec{k}'}\}. Note that the sums over \vec{k} in Eq. (4) only go over half the Brillouin zone (BZ); a convenient choice of the BZ is given by a rhombus whose vertices lie at $(k_x, k_y) = (\pm 2\pi, 0)$ and $(0, \pm 2\pi/\sqrt{3})$. The Hamiltonian in Eq. (3) can then be written in momentum space as$

$$H = \sum_{\vec{k} \in \frac{1}{2}\text{BZ}} \begin{pmatrix} \hat{a}_{\vec{k}}^\dagger & \hat{b}_{\vec{k}}^\dagger \end{pmatrix} H_k \begin{pmatrix} \hat{a}_{\vec{k}} \\ \hat{b}_{\vec{k}} \end{pmatrix},$$

$$H_{\vec{k}} = 2[J_1 \sin(\vec{k} \cdot \vec{M}_1) - J_2 \sin(\vec{k} \cdot \vec{M}_2)]\tau^x + 2[J_3 + J_1 \cos(\vec{k} \cdot \vec{M}_1) + J_2 \cos(\vec{k} \cdot \vec{M}_2)]\tau^y, \quad (5)$$

where τ^a are Pauli matrices denoting pseudospin. The dispersion relation can be derived from Eq. (5); it consists of two bands with energies

$$E_{\vec{k}}^\pm = \pm 2[\{J_1 \sin(\vec{k} \cdot \vec{M}_1) - J_2 \sin(\vec{k} \cdot \vec{M}_2)\}^2 + \{J_3 + J_1 \cos(\vec{k} \cdot \vec{M}_1) + J_2 \cos(\vec{k} \cdot \vec{M}_2)\}^2]^{1/2}. \quad (6)$$

The phase diagram of the model can be deduced from Eq. (6). Given that $J_i \geq 0$, it is convenient to normalize them so that $J_1 + J_2 + J_3 = 1$. This describes points lying within (or on) an equilateral triangle. This triangle can be divided into four smaller equilateral triangles as shown in Fig. 3, namely, A_x where $J_1 > J_2 + J_3$, A_y where $J_2 > J_1 + J_3$, A_z where $J_3 > J_1 + J_2$, and B where each of the J_i is less than the sum of the other two. It turns out⁴ that the system is gapped in the three A phases, with $E_{\vec{k}}$ being non-zero for all \vec{k} , and is gapless in the B phase, with $E_{\vec{k}} = 0$ for some value of \vec{k} whose value depends on the location of the point in that phase. The four phases are separated from each other by quantum critical lines where one of the couplings is equal to the sum of the other two.

III. PHASE DIAGRAM FOR EDGE STATES

In this section, we will consider two kinds of edges for the honeycomb lattice, namely, zigzag and armchair^{80,81}. These are shown in Figs. 2 and 4 respectively. We will assume that the edges are infinitely long; translational invariance then implies that the edge states can be labeled by their momentum k . We will analytically study the ranges of the couplings J_i for which edge states exist for these two kinds of edges. (In principle there can be more complicated kinds of edges, but analytical results for the edge states are then no longer available).

To find the edge states, we first write the Hamiltonian in Eq. (3) in the form

$$H = 2i \sum_{\alpha\beta} \hat{b}_\beta L_{\beta\alpha} \hat{a}_\alpha, \quad (7)$$

where α, β label the sites, and $L_{\alpha\beta}$ is a real matrix. We now use the Heisenberg equations of motion

$d\hat{a}_\alpha/dt = i[H, \hat{a}_\alpha]$ and similarly for \hat{b}_β . We then obtain

$$\frac{d\hat{a}_\alpha}{dt} = -4 \sum_\beta \hat{b}_\beta L_{\beta\alpha},$$

$$\frac{d\hat{b}_\beta}{dt} = 4 \sum_\alpha L_{\beta\alpha} \hat{a}_\alpha. \quad (8)$$

We note that the Hamiltonian in Eq. (7) and the time evolution given in Eqs. (8) are invariant under an effective time-reversal transformation which complex conjugates all numbers, and takes $t \rightarrow -t$, $\hat{a}_\alpha \rightarrow \hat{a}_\alpha$ and $\hat{b}_\beta \rightarrow -\hat{b}_\beta$ ^{77,85}. Such a symmetry ensures that all the zero energy modes (to be discussed below) involve only the \hat{a} operators or only the \hat{b} operators, not combinations of the two. Thus all the edge states, in contrast to their bulk counterparts, have weights on either A or B sublattices of the honeycomb, but not both.

We will now see that for appropriate ranges of couplings, there are states which have zero energy and are localized near a particular edge. We note that our analysis is similar to that used to find edge states in graphene^{80,81} and other systems^{82,83}, except that we are considering Majorana fermions rather than ordinary fermions⁸⁴. We will find the wave functions of these states by solving Eqs. (8). We will henceforth denote wave functions by alphabets without hats (such as a and b) to distinguish them from operators which are denoted by \hat{a} and \hat{b} .

A. Zigzag Edge

We look for a state with momentum k at the zigzag edge at the top of a system as shown in Fig. 2; k lies in the range $-\pi$ to π . In that figure, the wave functions for the Majorana operators of type \hat{b} are given by $b_{m,n}$, where n goes from $-\infty$ to ∞ and increases towards the right along the edge, and $m = 1, 2, 3, \dots$ increases as we go down away from the edge and into the bulk of the system. Further, we will take $b_{m,n} = b_m e^{ikn}$ or $b_m e^{ik(n+1/2)}$ depending on whether m is odd or even. Similarly, the wave functions for Majorana operators of type \hat{a} are given by $a_{m,n} = a_m e^{ikn}$ or $a_m e^{ik(n+1/2)}$; these factors are not shown in Fig. 2.

We then discover that the Heisenberg equations of motion in Eqs. (8) have zero energy solutions (i.e., with $d\hat{a}_\alpha/dt = 0$ and $d\hat{b}_\beta/dt = 0$) in which $a_m = 0$ for all m , and

$$J_1 b_m e^{ikn} + J_2 b_m e^{ik(n+1)} + J_3 b_{m+1} e^{ik(n+\frac{1}{2})} = 0 \quad (9)$$

for all $m \geq 1$. This is solved by assuming that $b_m = (\lambda_k)^m$; we then get

$$\lambda_k = -\frac{J_1 e^{-ik/2} + J_2 e^{ik/2}}{J_3}. \quad (10)$$

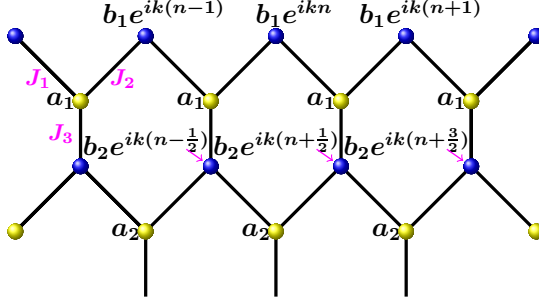


FIG. 2: (Color online) Zigzag edge. Majorana fermions with a momentum k along the edge are indicated.

For a normalizable edge state, we require $|\lambda_k| < 1$. According to Eq. (10) this occurs if

$$\cos k < \frac{J_3^2 - J_1^2 - J_2^2}{2J_1J_2}. \quad (11)$$

We discover that Eq. (11) is valid for all values of k in region A_z and for a finite range of values of k in region B . Since Eq. (11) has a solution with $-k$ if it has a solution with $+k$, and $\lambda_{-k} = \lambda_k^*$ according to Eq. (10), we can superpose these two wave functions (along with appropriate creation and annihilation operators) to obtain a Hermitian solution for $\hat{b}_{m,n}$ of the form $e^{ikn}(\lambda_k)^m \hat{b}_k + e^{-ikn}(\lambda_{-k})^m \hat{b}_k^\dagger$. (For $k = 0$ we directly get a real wave function of the form λ_0^m , where $\lambda_0 = -(J_1 + J_2)/J_3$, and therefore a Hermitian solution of the form $\lambda_0^m \hat{b}_0$; such a state exists everywhere in region A_z). In regions A_x and A_y , Eq. (11) is not satisfied for any value of k ; hence there are no zigzag edge states in these two regions. Fig. 3 shows the phase diagram where Majorana states of type \hat{b} exist at a zigzag edge at the top edge of the system. The length scale over which an edge state decays into the bulk is given by $\xi_k = -1/\ln|\lambda_k|$.

A similar analysis shows that the zigzag edge at the bottom of the Kitaev system will have Majorana states of type \hat{a} (i.e., with $b_m = 0$ for all m) in the same regions as shown in Fig. 3. These statements assume that the top and bottom edge are separated by a distance which is much larger than the decay length ξ_k . If the separation between the edges is comparable to ξ_k for some value of k , the two edge states will hybridize to give two states with energies different from zero.

B. Armchair Edge

We now look for a state at an armchair edge with momentum k as shown in Fig. 4. The \hat{a} and \hat{b} Majorana operators have wave functions given by $a_m e^{ikn}$ and $b_m e^{ikn}$; the figure shows these factors only for b_m . Note that this figure is obtained by rotating Fig. 2 by $\pi/2$ so that the horizontal bonds have couplings J_3 in Fig. 4.

We find that the Heisenberg equations of motion have zero energy solutions with $a_m = 0$ for all m , provided

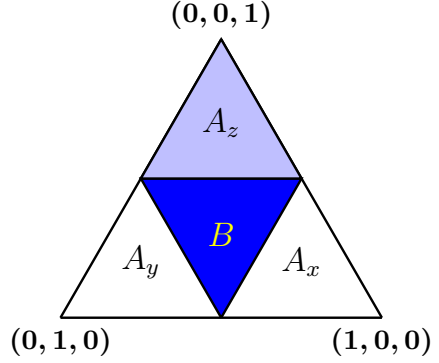


FIG. 3: (Color online) Phase diagram for zigzag edge states in the triangle with $J_1 + J_2 + J_3 = 1$. Majorana modes exist in the regions A_z and B .

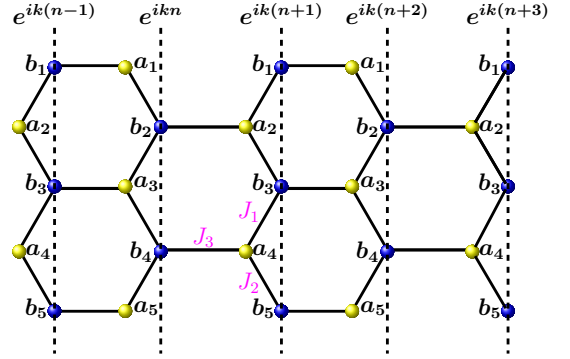


FIG. 4: (Color online) Armchair edge. Majorana fermions with a momentum k along the edge are indicated.

that

$$J_1 b_m + J_2 b_{m+2} + J_3 b_{m+1} e^{-ik} = 0 \quad (12)$$

for all $m \geq 1$, and

$$J_2 b_2 + J_3 b_1 e^{-ik} = 0. \quad (13)$$

Assuming $b_m = (\lambda_k)^m$, we get from Eq. (12)

$$\lambda_k^2 + \frac{J_3}{J_2} e^{-ik} \lambda_k + \frac{J_1}{J_2} = 0. \quad (14)$$

This has the solutions

$$\lambda_{k\pm} = \frac{1}{2J_2} \left[-J_3 e^{-ik} \pm \sqrt{J_3^2 e^{-2ik} - 4J_1J_2} \right]. \quad (15)$$

These two roots satisfy the equations

$$\lambda_{k+} + \lambda_{k-} = - (J_3/J_2) e^{-ik}, \quad (16)$$

$$\lambda_{k+} \lambda_{k-} = J_1/J_2. \quad (17)$$

Eqs. (12-13) imply that a normalizable edge state will exist if both $|\lambda_{k\pm}| < 1$. Eq. (17) then implies that we must

have $J_1 < J_2$. This condition and $|\lambda_{k\pm}| < 1$ together imply that $|\lambda_{k+} + \lambda_{k-}| \leq 1 + (J_1/J_2)$. Substituting this in Eq. (16), we obtain the condition $J_3 \leq J_1 + J_2$. Putting these together with $J_1 < J_2$, we obtain the dark shaded region on the left side of Fig. 5 where zero energy edge modes of type \hat{b} exist for some values of k . Combining states with $\pm k$ will again give us Majorana operators which are Hermitian. A similar analysis shows that zero energy edge modes of type \hat{a} (i.e., with $b_m = 0$ for all m) exist in the light shaded region on the right side of Fig. 5, namely, in the region with $J_2 < J_1$ and $J_3 \leq J_1 + J_2$.

Before ending this subsection, we note that the solution we have found for a zigzag edge state is an extension of the one in standard graphene with isotropic hoppings⁸⁰; the complex version of our solution corresponding to a single value of the momentum k (rather than a Hermitian superposition of $\pm k$) reproduces the graphene edge state for the special case $J_1 = J_2 = J_3$. For an armchair edge, on the other hand, there is no solution for $J_1 = J_2 = J_3$ and therefore no solution in standard graphene. However, armchair edge states can be found for strained graphene with anisotropic hoppings⁸¹.

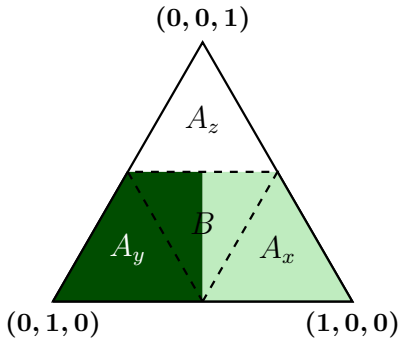


FIG. 5: (Color online) Phase diagram for armchair edge states in the triangle with $J_1 + J_2 + J_3 = 1$. Majorana modes of type \hat{b} (\hat{a}) exist in the regions A_y (A_x) and the left (right) half of B . These regions are indicated by dark (light) shades.

C. Finite Systems

In Secs. III A and III B, we considered systems whose edges are infinitely long and are therefore translationally invariant. This allowed us to effectively map the system to a 1D problem which is characterized by the parameters J_i and the edge momentum k .

In this section, we will numerically study finite systems which are not translationally invariant. We consider a system which has zigzag edges along the x direction and armchair edges along the y direction. Specifically, we consider a system with $N_x \times N_y = 27 \times 14$ sites, with $J_1 = 0.7$, $J_2 = 0.15$ and $J_3 = 0.15$; this lies in the region A_x in the phase diagram in Fig. 5. For these parameter values, the discussion in the previous subsection implies that there should be edge modes on the armchair edges.

These will not be at exactly zero energy due to hybridization between the two armchair edges on the opposite sides of the system. However, we find that their energies are quite close to zero since the distance between the two edges is $N_x = 27$ is much larger than the lattice spacing; we will therefore continue to call them Majorana modes. Numerically we find a total of 14 Majorana edge modes. This agrees with what we expect from Fig. 4; on each of the armchair edges, the number of Majorana modes should be equal to the number of either a or b sites, and this number is equal to $N_y/2 = 7$. Interestingly, if we look at the wave functions of all the edge modes, we find that 12 of them are localized along the armchair edges as expected (see Fig. 6 for an example), but the remaining 2 are localized at the corners as shown in Fig. 7.

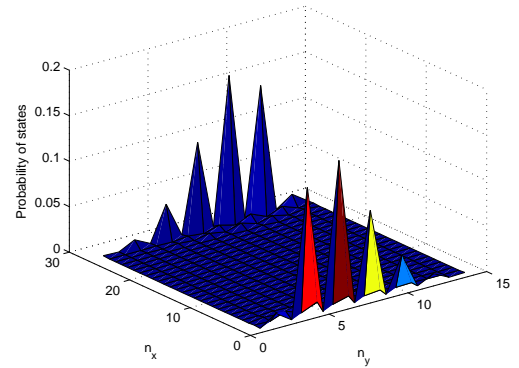


FIG. 6: (Color online) Armchair edge states for a system with $N_x \times N_y = 27 \times 14$ sites, with $J_1 = 0.7$, $J_2 = 0.15$ and $J_3 = 0.15$.

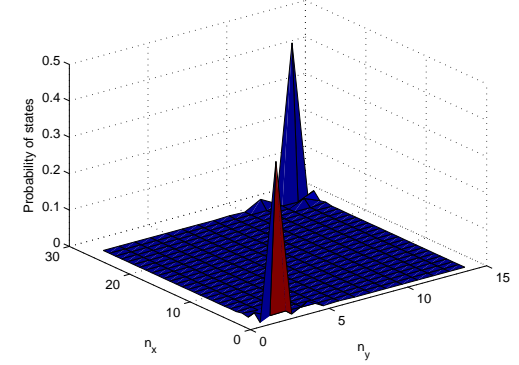


FIG. 7: (Color online) Corner states for a system with $N_x \times N_y = 27 \times 14$ sites, with $J_1 = 0.7$, $J_2 = 0.15$ and $J_3 = 0.15$.

Let us now consider the same 27×14 system but change the couplings to $J_1 = 1/6$, $J_2 = 1/6$ and $J_3 = 2/3$. According to Fig. 3, this lies in the A_z phase and should therefore only have states on the zigzag edges. Indeed we find numerically that there are 26 edge states; of these 13 are at the top zigzag edge and 13 are at the bottom

zigzag edge. This is expected since the top (bottom) row with 27 sites has 13 sites of type \hat{b} (\hat{a}).

D. Properties of the edge states

From the numerical studies of the previous subsection and from general analytical results obtained in earlier subsections, we have confirmed that the number of edge modes is exactly half the number of sites at the edge for an armchair edge. This fact is reminiscent of the edge states at the ends of unconventional superconductors for which one finds exactly half the number of states as the number of transverse momentum modes⁸⁸. In this section, we explore this property a little further. To this end, let us consider a zigzag edge and define a two-component fermion for a semi-infinite 2D Kitaev model $\hat{\psi}_{m,k}^\dagger = [\hat{a}_{m,k}^\dagger, \hat{b}_{m,k}^\dagger]$, where k denotes the momentum along the edge and m denotes the coordinate in the direction perpendicular to the edge (see Fig. 2). (The operators $\hat{a}_{m,k}^\dagger$ and $\hat{b}_{m,k}^\dagger$ are obtained by Fourier transforming $\hat{a}_{m,n}$ and $\hat{b}_{m,n}$ as explained below). We then define a correlation matrix C whose elements are given by

$$\begin{aligned} C_{11} &= \sum_m \langle \hat{a}_{m,k}^\dagger \hat{a}_{m,k} + \hat{b}_{m,k}^\dagger \hat{b}_{m,k} \rangle, \\ C_{12} &= C_{21} = \sum_m \langle i\hat{a}_{m,k}^\dagger \hat{b}_{m,k} - i\hat{b}_{m,k}^\dagger \hat{a}_{m,k} \rangle, \\ C_{22} &= \sum_m \langle \hat{a}_{m,k}^\dagger \hat{a}_{m,k} - \hat{b}_{m,k}^\dagger \hat{b}_{m,k} \rangle, \end{aligned} \quad (18)$$

where $\langle \dots \rangle$ implies properly normalized sums over m and is taken with respect to a state with a fixed energy and momentum k .

Let us evaluate the matrix C for the bulk states in the limit of large J_3 . In this limit the diagonal elements can be shown to be zero (to show this we have to ignore a constant which comes from on-site terms like $\hat{a}_{m,n}^2 = \hat{b}_{m,n}^2 = 1$, as explained after Eq. (25)), while the off-diagonal elements give ± 1 if the state is occupied; hence the eigenvalues λ_i of C are ± 1 . In contrast, for a Majorana mode localized at one of the edges (on, say, the A sublattice), the off-diagonal components are zero while the diagonal components yield 1 so that C has doubly degenerate eigenvalue $\lambda_1 = \lambda_2 = 1$ for these states. For a Majorana mode localized at the other edge on the B sublattice, the diagonal components and hence the eigenvalues are ± 1 . Thus, for all single Majorana occupied states, edge or bulk, the eigenvalues of C assume integer values. These results can be easily extended for all values of the couplings J_i .

Let us now consider a situation where a Kitaev system is in a gapped phase with localized zero energy edge states present at the zigzag edges, on one sublattice at the top edge and the other sublattice on the bottom edge; the two edges are assumed to be very far from each other. Let

us consider tunneling a bulk Majorana fermion from another Kitaev system (which is gapless) with zero energy and wave function $(u, v) = (1, 1) \exp[i(k_1 m + k_2 n)]/\sqrt{2}$. Since the zero energy states of the gapped Kitaev system only reside at the edges, the Majorana fermion must, after tunneling, divide between the two zigzag edges. Thus the state of the Majorana particle must have the form $|\psi\rangle = \alpha|A\rangle + \beta|B\rangle$ where $|A\rangle$ is a wave function localized along one edge with weight only on the A sublattice and $|B\rangle$ is localized along the other edge with weight only on the B sublattice. In the absence of any perturbations which break sublattice symmetry, we will have $|\alpha|^2 = |\beta|^2 = 1/2$. For this state, we will have $C_{12} = C_{21} = 0$ (since the edges are far from each other), while $C_{11} = 1$ and $C_{22} = 0$; this again leads to integer eigenvalues. Thus for any Majorana state, the eigenvalues of C will always be a positive or negative integer; for an unoccupied Majorana state, $C = 0$ by definition. Thus the behavior of the $|\lambda_i|$ is analogous to the properties of the expectation value of the number operator for fermions. The fluctuations to this expectation value can also be calculated and shown to vanish.

Next we consider a local correlation where the sum over m for the elements of C is taken over a finite number of lattice sites starting from a given edge; we choose the finite number to be much larger than the decay lengths of all the Majorana modes localized at that edge. Let us define the corresponding matrix as C' . Then for a split Majorana one has $C'_{11} = 1/2$, $C'_{22} = \pm 1/2$ [where the $(+/-)$ sign corresponds to the state localized at that edge having weights on the $A(B)$ sublattice respectively], and $C'_{12} = C'_{21} = 0$. This leads to fractional eigenvalues for C' . Thus the edge states of the Kitaev model provide us with a way of spatially separating the two sublattice components of the Majorana wave function leading to fractional expectation values for local correlation functions. One can easily show that the number operator for fermions constructed out of the Majorana will also have half-integer expectation value. However, the difference between the present situation and the well-known example of electron fractionalization found in the literature⁸⁹ (in the context of polyacetylene and quantum field theoretic models in one dimension) is that the fluctuations from this expectation value are not small here. We will show below that these states have either $\langle (\hat{a}_{m,k}^\dagger \hat{a}_{m,k})^2 \rangle = 1/2$ or $\langle (\hat{b}_{m,k}^\dagger \hat{b}_{m,k})^2 \rangle = 1/2$ depending on whether the states have weight on the A or B sublattice, and that there is a finite variance which signifies large fluctuations from the expectation value. Thus the fractionalization of the expectation value does not amount to fractionalization of the eigenvalues of the correlation matrix of the Majorana fermions.

The difference of the present situation from the standard electron fractionalization found in the literature⁸⁹ can be understood in a number of ways. In the limit of large J_3 , the Majorana modes near the top zigzag edge in Fig. 2 are completely localized at the sites of the top row labeled as $b_{1,n}$, while the Majorana modes near the bot-

tom zigzag edge are completely localized at the sites of the bottom row labeled as $a_{N_y,n}$, where N_y is the width of the system assumed to be much larger than 1. Let us introduce the Fourier transform of the operators $b_{1,n}$ as

$$\hat{b}_{1,n} = \int_0^\pi \frac{dk}{2\pi} [\hat{b}_{1,k} e^{ikn} + \hat{b}_{1,k}^\dagger e^{-ikn}], \quad (19)$$

The inverse of this is given by

$$\begin{aligned} \hat{b}_{1,k} &= \sum_{n=-\infty}^{\infty} \hat{b}_{1,n} e^{-ikn}, \\ \hat{b}_{1,k}^\dagger &= \sum_{n=-\infty}^{\infty} \hat{b}_{1,n} e^{ikn}. \end{aligned} \quad (20)$$

We can similarly define Fourier transforms of the operators $a_{N_y,n}$, called $a_{N_y,k}$. Next, we have to find the ground state of the system. Since the modes labeled by $b_{1,k}$ and $a_{N_y,k}$ have zero energy for all values of k if J_3 is infinitely large, the ground state has an enormous degeneracy. To break this degeneracy, let us assume that J_1 and J_2 are slightly different from zero. This will introduce a small tunneling between the top and bottom rows of the form

$$\Delta H = \int_0^\pi \frac{dk}{2\pi} [\gamma_k \hat{b}_{1,k}^\dagger \hat{a}_{N_y,k} + h.c.], \quad (21)$$

where γ_k is the tunneling amplitude which is exponentially small: $\gamma_k \sim e^{-N_y/\xi_k}$, where ξ_k is the decay length of the mode k . The Hamiltonian in Eq. (21) has a unique ground state of the form

$$|gs\rangle = \prod_k (u_k \hat{b}_{1,k}^\dagger + v_k \hat{a}_{N_y,k}^\dagger) |vac\rangle, \quad (22)$$

where $|u_k|^2 = |v_k|^2 = 1/2$. We now see that at the top edge,

$$\langle gs | \hat{b}_{1,k}^\dagger \hat{b}_{1,k} | gs \rangle = \langle gs | (\hat{b}_{1,k}^\dagger \hat{b}_{1,k})^2 | gs \rangle = 1/2, \quad (23)$$

implying that the variance, $\langle gs | (\hat{b}_{1,k}^\dagger \hat{b}_{1,k})^2 | gs \rangle - \langle gs | \hat{b}_{1,k}^\dagger \hat{b}_{1,k} | gs \rangle^2 = 1/4$, is not small.

Another difference between Majorana fermions and standard electrons is as follows. The operator appearing in the diagonal component of Eq. (18), restricted to the top row given by $m = 1$ in Fig. 2, is given by

$$\hat{b}_{1,k}^\dagger \hat{b}_{1,k} = \sum_{n,n'=-\infty}^{\infty} \hat{b}_{1,n} \hat{b}_{1,n'} e^{ik(n-n')}, \quad (24)$$

which involves operators which are extremely non-local in space. Even if Eq. (24) is integrated over k , we still get a non-local expression

$$\int_0^\pi \frac{dk}{2\pi} \hat{b}_{1,k}^\dagger \hat{b}_{1,k} = -\frac{2i}{\pi} \sum_{n=-\infty}^{\infty} \sum_{r=0}^{\infty} \frac{\hat{b}_{1,n} \hat{b}_{1,n+2r+1}}{2r+1}, \quad (25)$$

plus an infinite constant coming from $\hat{b}_{1m}^2 = 1$. The non-local form originates from the fact that k is integrated over only half the Brillouin zone, i.e., $0 \leq k \leq \pi$. This, in turn, arises from the fact that the $\hat{b}_{1,k}$ are Fourier transforms of $\hat{b}_{1,n}$ which are Hermitian operators, namely, the Majorana fermions are indistinguishable from their antiparticles. The expression in Eq. (25) is to be contrasted with the total number operator for electrons which is always given by a sum over operators which are local in space.

The above arguments for the fractionalization of expectation values and the non-locality of Majorana modes at zigzag edges will hold at all points in the phase A_z in Fig. 3. We have shown in Sec. III A that there are Majorana modes near both the zigzag edges but residing entirely on opposite sublattices, for all values of k lying in the range $[0, \pi]$. If we choose the finite number of lattices in the definition of the local correlation C' to be much larger than the decay length ξ_k for all values of k , the eigenvalues of C' will be $\pm 1/2$.

IV. FLOQUET EVOLUTION

We will now consider what happens when the Hamiltonian varies periodically in time with a time period T^{77} . Namely, we will assume that the matrix L in Eq. (7) changes with time in such a way that $L(t+T) = L(t)$. Eqs. (8) and their solution can be written as matrix equations as follows. Given a system with $N = N_x N_y$ sites, let us introduce a $(2N)$ -dimensional column called \hat{c} whose first N entries are given by $(\hat{a}_1, \hat{a}_2, \dots, \hat{a}_N)^T$ and last N entries are given by $(\hat{b}_1, \hat{b}_2, \dots, \hat{b}_N)^T$. Given the N -dimensional matrix L , we define a $(2N)$ -dimensional real antisymmetric matrix M by the block form

$$M = \begin{pmatrix} 0 & -LT \\ L & 0 \end{pmatrix}. \quad (26)$$

Eqs. (8) can then be written as $d\hat{c}(t)/dt = 4M(t)\hat{c}(t)$. The periodicity of $M(t)$ in time implies that the solution of this equation is given by

$$\begin{aligned} \hat{c}(T) &= U(T, 0) \hat{c}(0), \\ \text{where } U(T, 0) &= \mathcal{T} e^{4 \int_0^T dt M(t)}, \end{aligned} \quad (27)$$

and \mathcal{T} denotes the time-ordering symbol. $U(T, 0)$ is called the Floquet operator. It is a unitary matrix (in our case it is real and orthogonal), and it can be computed numerically for a given form of $M(t)$.

The eigenvalues of $U(T, 0)$, called Floquet eigenvalues (FE), are given by phases, $e^{i\theta_j}$, and they come in complex conjugate pairs if $e^{i\theta_j} \neq \pm 1$. If $U(T, 0)$ has eigenvalues ± 1 , the corresponding eigenvectors can be shown to be real.

In the next section, we will present our results for eigenvectors of $U(T, 0)$ which are localized near the edges of the honeycomb lattice and whose FE are equal to ± 1 .

In order to find these edge modes, we will use the same numerical methods as in Ref. 77. Namely, we will first use the inverse participation ratio to identify eigenvectors of the Floquet operator which are localized near the edges. [Given an eigenvector ψ_j , normalized so that $\sum_{m=1}^{2N} |\psi_j(m)|^2 = 1$, we define its inverse participation ratio as $I_j = \sum_{m=1}^{2N} |\psi_j(m)|^4$. Eigenvectors with larger values of I_j are more localized in space]. We will then check if these eigenvectors are real and if their FE (± 1) are separated from all the other FE by a finite gap as the dimensions of the system, N_x and N_y , are made very large. If all these conditions are met, these eigenvectors will be called Floquet Majorana modes.

V. PERIODIC δ -FUNCTION KICKS

In this section, we will study what happens when one of the parameters in the Kitaev honeycomb model is given δ -function kicks periodically in time. The reason for studying this kind of a periodic variation is that it is easy to study both numerically and analytically⁸⁶.

Let us first consider what happens if J_3 in Eq. (3) is periodically kicked, so that

$$J_3(t) = J_0 + J_p \sum_{n=-\infty}^{\infty} \delta(t - nT), \quad (28)$$

where the time period T is related to the drive frequency as $T = 2\pi/\omega$.

We numerically compute the operator $U(T, 0)$ for various values of the parameters $J_1, J_2, J_0, J_p, \omega$ and the system size $N_x \times N_y$. We then find all the eigenvalues and eigenvectors of $U(T, 0)$ and use the inverse participation ratio and the eigenvectors to identify the Floquet Majorana modes as described above.

The Floquet operator is given by a product of two exponentials

$$U(T, 0) = e^{4M_1} e^{4M_0 T}, \quad (29)$$

where $e^{4M_0 T}$ is the operator which time evolves from $t = 0$ to $t = T$, and e^{4M_1} then evolves across the δ -function at $t = T$.

To illustrate the Floquet Majorana modes, we now consider a system with $N_x \times N_y = 27 \times 14$ sites with $J_1 = 0.7, J_2 = 0.15, J_0 = 0.15, J_p = 0.2$, and $\omega = 3$. We discover numerically that there are 50 Floquet edge modes; of these, 14 have FE very close to $+1$ and 36 have FE very close to -1 . Further, we discover that there are Floquet modes on both zigzag and armchair edges. (An example of a Floquet zigzag edge mode is shown in Fig. 8). This is in contrast to the time-independent version of the model discussed in Sec. III C which has only 14 Majorana edge modes, all of which lie on the armchair edges.

The appearance of Floquet modes on both kinds of edges in this system can be understood as follows. As discussed in Sec. III, the system with the time-independent

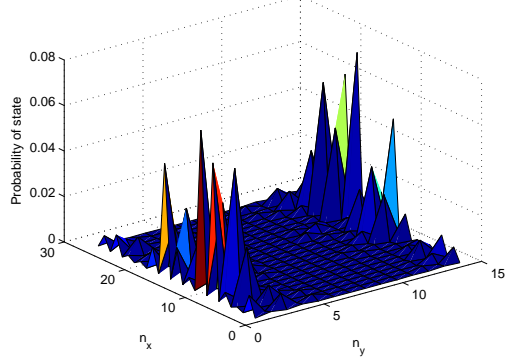


FIG. 8: (Color online) Zigzag edge states for a system with $N_x \times N_y = 27 \times 14, J_1 = 0.7, J_2 = 0.15, J_0 = 0.15, J_p = 0.2$ and $\omega = 3$.

part of the Hamiltonian (i.e., with $J_3 = J_0$) lies in the A_x phase and therefore has Majorana modes only on armchair edges or at corners as shown in Figs. 6-7. At the times $t = nT$, Eq. (28) shows that J_3 is infinitely large; if the couplings are normalized to satisfy $J_1 + J_2 + J_3 = 1$, the system at these times will lie at the top vertex $(0, 0, 1)$ in Fig. 3 and should therefore have Majorana modes on zigzag edges. We therefore expect the kicked system to have Majorana modes on both edges.

A. Relation between bulk and edge modes

We can understand the Floquet Majorana modes at the edges from the properties of the bulk modes as follows. For the infinite system with translation symmetry, the modes $(\hat{a}_{\vec{k}}, \hat{b}_{\vec{k}})$ with different values of \vec{k} decouple from each other; hence we can study the Floquet operator $U_{\vec{k}}(T, 0)$ for each \vec{k} separately. We then see from Eq. (5) that

$$\begin{aligned} U_{\vec{k}}(T, 0) &= e^{-i2J_p \tau^y} e^{-iT(X_{\vec{k}} \tau^z + Y_{\vec{k}} \tau^y)}, \\ X_{\vec{k}} &= 2 [J_1 \sin(\vec{k} \cdot \vec{M}_1) - J_2 \sin(\vec{k} \cdot \vec{M}_2)], \\ Y_{\vec{k}} &= 2 [J_0 + J_1 \cos(\vec{k} \cdot \vec{M}_1) + J_2 \cos(\vec{k} \cdot \vec{M}_2)]. \end{aligned} \quad (30)$$

We will assume that $2J_p/\pi$ is not equal to an integer. According to Ref. 77, a Majorana edge mode should appear or disappear when $U_{\vec{k}}(T, 0)$ has FE equal to ± 1 . The structure of Eq. (30) implies that this will happen if

$$J_1 \sin(\vec{k} \cdot \vec{M}_1) - J_2 \sin(\vec{k} \cdot \vec{M}_2) = 0, \quad (31)$$

and

$$2J_p + 2T \left[J_0 + J_1 \cos(\vec{k} \cdot \vec{M}_1) + J_2 \cos(\vec{k} \cdot \vec{M}_2) \right] = n\pi, \quad (32)$$

where n is an integer. $[U_{\vec{k}}(T, 0)]$ will have a FE equal to $+1$ (-1) if n is even (odd). We can use Eqs. (31-32) to

find the critical values of $\omega_{\vec{k}}$ where Majorana edge modes appear or disappear. Since

$$\begin{aligned} & [(J_1 \sin(\vec{k} \cdot \vec{M}_1) - J_2 \sin(\vec{k} \cdot \vec{M}_2))^2 \\ & + [J_1 \cos(\vec{k} \cdot \vec{M}_1) + J_2 \cos(\vec{k} \cdot \vec{M}_2)]^2 \\ & = J_1^2 + J_2^2 + 2J_1 J_2 \cos(k_x), \end{aligned} \quad (33)$$

Eq. (31) implies that

$$\begin{aligned} & J_1 \cos(\vec{k} \cdot \vec{M}_1) + J_2 \cos(\vec{k} \cdot \vec{M}_2) \\ & = \pm \sqrt{J_1^2 + J_2^2 + 2J_1 J_2 \cos(k_x)}. \end{aligned} \quad (34)$$

Then Eq. (32) implies that the critical values of $\omega = 2\pi/T$ are given by

$$\omega_{\vec{k}} = \frac{4\pi [J_0 \pm \sqrt{J_1^2 + J_2^2 + 2J_1 J_2 \cos(k_x)}]}{n\pi - 2J_p} \quad (35)$$

which depends on a single momentum k_x . For a system with a finite width bounded by infinitely long zigzag edges along the x direction, the momentum k shown in Fig. 2 is equal to k_x . We therefore have the prediction that for such a finite system, Floquet Majorana modes should appear or disappear at the edges with a given value of k at frequencies which are given by Eq. (35). Further, the Majorana mode should have a FE equal to $(-1)^n$.

This result can be generalized to systems in arbitrary dimensions. Let us consider a d -dimensional system in which there are pairs of modes with momenta \vec{k} which are governed by a Hamiltonian of the form

$$H'_{\vec{k}} = 2[\epsilon_{\vec{k}} \tau^y + \Delta_{\vec{k}} \tau^z], \quad (36)$$

where a component of $\epsilon_{\vec{k}}$ changes due to periodic kicks with a frequency ω . Let $\epsilon_{1\vec{k}}$ and $\epsilon_{0\vec{k}}$ be the values of $\epsilon_{\vec{k}}$ during and between the kicks. The Floquet operator is then given by

$$U_{\vec{k}}(T, 0) = e^{-i2\epsilon_{1\vec{k}}\tau^y} e^{-i2T(\Delta_{\vec{k}}\tau^z + \epsilon_{0\vec{k}}\tau^y)}. \quad (37)$$

If $2\epsilon_{1\vec{k}}/\pi$ is not equal to an integer, we can show that $U_{\vec{k}}(T, 0)$ can have FE equal to ± 1 only if $\Delta_{\vec{k}} = 0$. Next, $\Delta_{\vec{k}} = 0$ will generally define a $(d-1)$ -dimensional hypersurface of the d -dimensional Brillouin zone. Hence the frequency at which Majorana modes will appear or disappear, $\omega_{\vec{k}}$, will depend on $d-1$ momenta and will be determined by the conditions

$$\begin{aligned} \Delta_{\vec{k}} &= 0, \\ \omega_{\vec{k}} &= 4\pi\epsilon_{0\vec{k}}/(n\pi - 2\epsilon_{1\vec{k}}), \end{aligned} \quad (38)$$

where n is an integer. If we consider a system with a finite width which is bounded by two infinitely large $(d-1)$ -dimensional surfaces, there will generally be Floquet Majorana modes on these surfaces which are parameterized by $d-1$ momenta. Eq. (38) will then determine the frequencies at which these modes (with FE equal to $(-1)^n$)

appear or disappear. For instance, the 2D Kitaev model has $d=2$ so that the Floquet Majorana modes and the critical frequencies $\omega_{\vec{k}}$ depend on a single momentum, while the 1D Ising model or Kitaev chain has $d=1$ so that the Majorana modes and the critical frequencies are independent of any momentum⁷⁷.

In the next subsection, we will use the above ideas to arrive at a better understanding of the Floquet Majorana modes by mapping the Kitaev honeycomb model to the 1D Kitaev chain where the Floquet problem has been studied in detail earlier⁷⁷.

B. Mapping from the honeycomb model to a one-dimensional chain

Consider a system which has a finite width in the y -direction (with zigzag edges along the top and bottom as indicated in Fig. 2) and is infinitely long in the x -direction. The momentum k along the x -axis is a good quantum number. We now use the Heisenberg equations of motion

$$\begin{aligned} \frac{d\hat{a}_m}{dt} &= (J_1 e^{-ik/2} + J_2 e^{ik/2}) \hat{b}_m + J_3 \hat{b}_{m+1}, \\ \frac{d\hat{b}_m}{dt} &= -(J_1 e^{ik/2} + J_2 e^{-ik/2}) \hat{a}_m - J_3 \hat{a}_{m-1}, \end{aligned} \quad (39)$$

for all $m \geq 1$, with the understanding that $\hat{a}_0 = 0$.

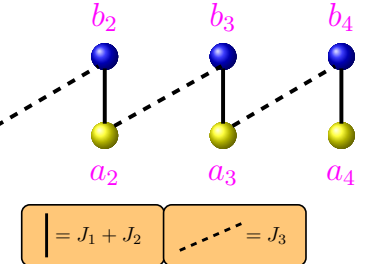


FIG. 9: (Color online) Mapping from the Kitaev honeycomb model to a one-dimensional chain for $k=0$, with the $J_1 + J_2$ couplings shown as solid lines and J_3 shown as dashed lines.

We first consider the case $k=0$. Then this problem converts in a straightforward way to a special case of the 1D Kitaev chain (a system of electrons with p -wave superconductivity) with couplings as shown in Fig. 9. This chain is described by the Hamiltonian^{77,85}

$$H = i \sum_{n=1}^{\infty} [-J_x \hat{b}_{n+1} \hat{a}_n - J_y \hat{b}_n \hat{a}_{n+1} + \mu \hat{b}_n \hat{a}_n]. \quad (40)$$

The Heisenberg equations of motion of the operators \hat{a}_n and \hat{b}_n in Eq. (40) agree with Eqs. (39) with $k=0$ if we set

$$J_x = J_3/2, \quad J_y = 0, \quad \text{and} \quad \mu = -(J_1 + J_2)/2. \quad (41)$$

Interestingly, this system is equivalent, by a Jordan-Wigner transformation⁸⁷, to an Ising model in a transverse magnetic field described by the Hamiltonian

$$H = - \sum_{n=1}^{\infty} [J_x \sigma_n^x \sigma_{n+1}^x + \mu \sigma_n^z]. \quad (42)$$

We now see that if J_3 is given periodic δ -function kicks in the honeycomb model, it corresponds, for $k = 0$, to a 1D model in which the parameter J_x is given periodic δ -function kicks without changing the values of μ and J_y . This problem has been studied in Ref. 77. It is known numerically (and analytically for the special case $J_0 = 0$) that the δ -function kicks can produce Floquet Majorana modes at the ends of the 1D system, which correspond to the zigzag edges of the 2D model. In fact, we find numerically that one Floquet Majorana mode appears at each of the zigzag edges (at the top and at the bottom of the 2D system) when the kicking frequency ω is taken to be very large.

Next, we consider what happens if $k \neq 0$. In this case, we can rewrite two of the parameters appearing in Eqs. (39) as

$$J_1 e^{\pm ik/2} + J_2 e^{\mp ik/2} = J_k e^{\pm i\phi_k},$$

where $J_k = \sqrt{J_1^2 + J_2^2 + 2J_1 J_2 \cos k}$. (43)

We can then show that the phase ϕ_k can be removed from Eqs. (39) by a unitary transformation; this unitary transformation is independent of J_3 and is therefore not affected by the periodic kicks in J_3 . We can therefore study the problem just as in the case with $k = 0$, except that the parameter μ in Eq. (41) is now given by $\mu_k = -J_k/2$. We thus have a family of 1D problems which are labeled by the parameter k . For each k , we look for Floquet edge modes. If we find such a mode, we can use the idea discussed in Secs. III A and III B for the time-independent problem to superpose the modes for the Floquet problems with $+k$ and $-k$ to obtain a Majorana mode with Hermitian operators.

We have used the procedure described above to numerically find the region in the space of ω (from 1 to 20) and k (from 0 to π) where Floquet Majorana modes appear. Fig. 10 shows this for a system with a width of 100 sites (i.e., the index m for a_m and b_m goes from 1 to 100), with $J_1 = 0.70$, $J_2 = 0.15$, $J_0 = 0.15$ and $J_p = 0.3$. If ω is sufficiently large, there is a Floquet Majorana mode with FE equal to +1. As ω is decreased, there is an empty region in which there are no Majorana modes for any k . As ω is decreased further, Majorana modes appear with FE equal to -1. As explained in more detail below, the figure also shows four red solid lines; two of these bound the empty region from the right and left, while the other two almost coincide and lie within the blue region. When ω is decreased below the last two lines, the Majorana mode with FE equal to -1 disappears and a mode with FE equal to +1 appears.

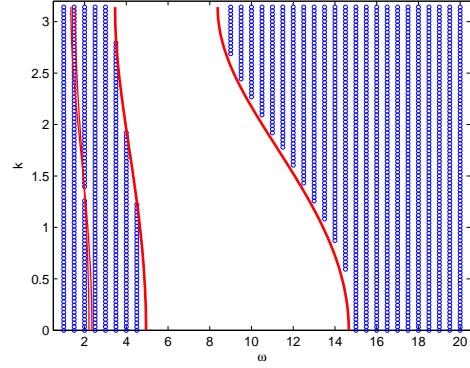


FIG. 10: (Color online) Blue regions in the (ω, k) space where Majorana states appear on the zigzag edges when the parameter J_3 is given periodic δ -function kicks. The system being considered has a width of 100 sites, and $J_1 = 0.7$, $J_2 = 0.15$, $J_0 = 0.15$ and $J_p = 0.3$. The empty region in the middle is bounded on the right and left by two solid red lines which show the analytical results given in Eqs. (45) and (46) respectively. Two more red solid lines corresponding to $n = -1$ and 2 are shown. They almost coincide with each other and appear within the blue regions on the left; they cross near $\omega = 2$ and $k \simeq 1.3$.

We now check how well these numerical results agree with the analysis given in the previous subsection. According to Eqs. (35) and (43), Floquet edge modes with a given momentum k and FE equal to $(-1)^n$ should appear or disappear when

$$\omega_k = \frac{4\pi [J_0 \pm J_k]}{n\pi - 2J_p}, \quad (44)$$

where n is an integer. As the kicking frequency ω is decreased, Eq. (44) gives the red solid line on the right side of the empty region in Fig. 10 where a Floquet edge mode disappears with $n = 0$, namely,

$$\omega_k = \frac{4\pi [J_k - J_0]}{2J_p}, \quad (45)$$

and the red solid line on the left side of the empty region in Fig. 10 where a Floquet edge mode appears with $n = 1$, namely,

$$\omega_k = \frac{4\pi [J_0 + J_k]}{\pi - 2J_p}. \quad (46)$$

In general, for $n \leq 0$, we have a line given by

$$\omega_k = \frac{4\pi [J_k - J_0]}{2J_p - n\pi}, \quad (47)$$

while for $n \geq 1$, we have a line given by

$$\omega_k = \frac{4\pi [J_0 + J_k]}{n\pi - 2J_p}, \quad (48)$$

where Majorana modes appear or disappear. Fig. 10 also show the red solid lines for $n = -1$ and 2. These appear within the blue regions; they cross near $\omega = 2$ and $k \simeq 1.3$ where we see a small gap indicating that there are no Majorana modes in that region. When ω is decreased below these two lines, the Majorana mode with FE equal to -1 disappears and a mode with FE equal to $+1$ appears. When ω is decreased even further, more modes start appearing which correspond to $n > 2$ and $n < -1$.

C. Periodic δ -function kicks in J_1 and J_2

We have also studied what happens if we consider a finite system and apply periodic kicks to J_1 or J_2 , rather than to J_3 . The time-independent part of the Hamiltonian has $J_1 = 0.7$, $J_2 = 0.15$ and $J_3 = 0.15$; such a system lies in the A_x phase and therefore only has edge states on armchair edges. A periodic kick in J_1 means that at times $t = nT$, the value of J_1 is infinitely larger than J_2 and J_3 ; hence the system lies at the vertex $(1, 0, 0)$ in Fig. 3 which also lies in the A_x phase. Similarly, a periodic kick in J_2 means that at $t = nT$, the value of J_2 is infinitely larger than J_1 and J_3 ; the system then lies at the vertex $(0, 1, 0)$ in Fig. 3 which lies in the A_y phase. In both cases, we only expect edge states on armchair edges.

For a system with $N_x \times N_y = 27 \times 14$ with a kick in J_1 or J_2 with amplitude $J_p = 0.2$ and frequency $\omega = 3$, we find numerically that there are 14 Floquet Majorana modes, of which 12 are on the armchair edges and 2 are at the corners. Thus the number and location of the Majorana modes remain exactly the same as in the time-independent case discussed in Sec. III C.

VI. CONCLUSIONS

In this work we have studied both equilibrium and Floquet edge modes of the Kitaev model on a honeycomb lattice. One reason for studying the Kitaev model is that it is the minimal model in two dimensions where one can study edge states and derive a number of analytical results. These results can be immediately applied to graphene for the following reason. Graphene has ordinary fermion operators c and c^\dagger which can be written in terms of two Majorana fermion operators m_i at each site, as $c = (1/2)(m_1 + im_2)$ and $c^\dagger = (1/2)(m_1 - im_2)$. The Hamiltonian of graphene then turns out to be equivalent to two decoupled copies of the Kitaev Hamiltonian (four copies if we include the electron spin in graphene). This implies that if edge states appear in the Kitaev model under some conditions, they must also appear in graphene under the same conditions.

We have discussed the known analytical solutions for the equilibrium zero energy modes localized at both zigzag and armchair edges. These solutions lead to a

phase diagram for the presence or absence of these modes and the possible values of their momentum along the edge. These states, in contrast to the bulk modes, have wave function weight on only one of the sublattices. We have pointed out that this property provides a way of spatially separating the sublattice constituents of a Majorana fermion and have discussed this phenomenon in the context of standard electron fractionalization found, for example, in polyacetylene and edges of unconventional superconductors.

Next we have studied the Floquet edge modes which appear in the Kitaev model when the coupling on the bonds perpendicular to the edge is varied in time as periodic δ -function kicks. Using a relation between the bulk and edge modes we have found a generic condition on the drive frequency of a d -dimensional integrable model which needs to be satisfied for the appearance or disappearance of these edge modes. We have verified this generic condition in the Kitaev model with a finite width by mapping it to a one-dimensional model of electrons with p -wave superconductivity (or an Ising chain in a transverse magnetic field). We have shown that the δ -function kicks can lead to a large number of Floquet edge modes, and that these modes can appear on certain edges even when there are no equilibrium Majorana modes on those edges. Finally, we have supplemented our analytical calculations with numerical analysis for finite-sized systems which confirms the above prediction for the drive frequencies. In the context of Floquet modes, our numerics shows that edge modes can appear both at the edges and the corners of a finite sample as the drive frequency is varied.

We summarize our most important results as follows.

- (i) Periodic driving of some of the couplings of the Kitaev model can give rise to edge states in certain regimes of couplings where the time-independent part of the Hamiltonian has no edge states.
- (ii) The driving frequencies at which Majorana edge modes appear or disappear in a two-dimensional system can be completely understood by mapping it to a one-dimensional system in which the edge momentum appears as one of the parameters of the model.

There are proposals for realizing the Kitaev model in systems of cold atoms trapped in optical lattices^{90–93}. It may therefore be possible to look for states localized at the edges of such systems, both at equilibrium and in the presence of periodic driving. In the latter case, it would be necessary to consider the effects of random noise and various relaxation mechanisms which may be present in the system^{53,56,77}.

Acknowledgments

For financial support, M.T. thanks CSIR, India and D.S. thanks DST, India for Project No. SR/S2/JCB-44/2010. The authors thank R. Shankar for stimulating

discussions on related topics.

¹ M. Z. Hasan and C. L. Kane, *Rev. Mod. Phys.* **82**, 3045 (2010).

² X.-L. Qi and S.-C. Zhang, *Rev. Mod. Phys.* **83**, 1057 (2011).

³ C. Nayak, S. H. Simon, A. Stern, M. Freedman, and S. Das Sarma, *Rev. Mod. Phys.* **80**, 1083 (2008).

⁴ A. Kitaev, *Ann. Phys.* **321**, 2 (2006).

⁵ H.-D. Chen and Z. Nussinov, *J. Phys. A* **41**, 075001 (2008); Z. Nussinov and G. Ortiz, *Phys. Rev. B* **77**, 064302 (2008); G. Baskaran, S. Mandal, and R. Shankar, *Phys. Rev. Lett.* **98**, 247201 (2007); D.-H. Lee, G.-M. Zhang, and T. Xiang, *Phys. Rev. Lett.* **99**, 196805 (2007).

⁶ K. P. Schmidt, S. Dusuel, and J. Vidal, *Phys. Rev. Lett.* **100**, 057208 (2008); S. Dusuel, K. P. Schmidt, and J. Vidal, *Phys. Rev. Lett.* **100**, 177204 (2008); J. Vidal, K. P. Schmidt, and S. Dusuel, *Phys. Rev. B* **78**, 245121 (2008).

⁷ G. Kells, A. T. Bolukbasi, V. Lahtinen, J. K. Slingerland, J. K. Pachos, and J. Vala, *Phys. Rev. Lett.* **101**, 240404 (2008); G. Kells, J. K. Slingerland, and J. Vala, *Phys. Rev. B* **80**, 125415 (2009).

⁸ G. Kells and J. Vala, *Phys. Rev. B* **82**, 125122 (2010).

⁹ A. Kitaev, *Physics-Uspekhi* **44**, 131 (2001), arXiv:cond-mat/0010440v2 (2000).

¹⁰ C. W. J. Beenakker, *Annu. Rev. Condens. Matter Phys.* **4**, 113 (2013).

¹¹ R. M. Lutchyn, J. D. Sau, and S. Das Sarma, *Phys. Rev. Lett.* **105**, 077001 (2010).

¹² Y. Oreg, G. Refael, and F. von Oppen, *Phys. Rev. Lett.* **105**, 177002 (2010).

¹³ L. Fidkowski, J. Alicea, N. H. Lindner, R. M. Lutchyn, and M. P. A. Fisher, *Phys. Rev. B* **85**, 245121 (2012).

¹⁴ A. C. Potter and P. A. Lee, *Phys. Rev. Lett.* **105**, 227003 (2010).

¹⁵ I. C. Fulga, F. Hassler, A. R. Akhmerov, and C. W. J. Beenakker, *Phys. Rev. B* **83**, 155429 (2011).

¹⁶ T. D. Stanescu, R. M. Lutchyn, and S. Das Sarma, *Phys. Rev. B* **84**, 144522 (2011).

¹⁷ S. Tewari and J. D. Sau, *Phys. Rev. Lett.* **109**, 150408 (2012).

¹⁸ M. Gibertini, F. Taddei, M. Polini, and R. Fazio, *Phys. Rev. B* **85**, 144525 (2012).

¹⁹ J. S. Lim, L. Serra, R. López, and R. Aguado, *Phys. Rev. B* **86**, 121103 (2012).

²⁰ M. Tezuka and N. Kawakami, *Phys. Rev. B* **85**, 140508(R) (2012).

²¹ R. Egger and K. Flensberg, *Phys. Rev. B* **85**, 235462 (2012).

²² S. Gangadharaiah, B. Braunecker, P. Simon, and D. Loss, *Phys. Rev. Lett.* **107**, 036801 (2011).

²³ E. Sela, A. Altland, and A. Rosch, *Phys. Rev. B* **84**, 085114 (2011).

²⁴ A. M. Lobos, R. M. Lutchyn, and S. Das Sarma, *Phys. Rev. Lett.* **109**, 146403 (2012).

²⁵ R. M. Lutchyn and M. P. A. Fisher, *Phys. Rev. B* **84**, 214528 (2011).

²⁶ A. M. Cook, M. M. Vazifeh, and M. Franz, *Phys. Rev. B* **86**, 155431 (2012).

²⁷ F. L. Pedrocchi, S. Chesi, S. Gangadharaiah, and D. Loss, *Phys. Rev. B* **86**, 205412 (2012).

²⁸ D. Sticlet, C. Bena, and P. Simon, *Phys. Rev. Lett.* **108**, 096802 (2012); D. Chevallier, D. Sticlet, P. Simon, and C. Bena, *Phys. Rev. B* **85**, 235307 (2012).

²⁹ P. San-Jose, E. Prada, and R. Aguado, *Phys. Rev. Lett.* **108**, 257001 (2012); E. Prada, P. San-Jose, and R. Aguado, *Phys. Rev. B* **86**, 180503 (2012).

³⁰ J. Klinovaja and D. Loss, *Phys. Rev. B* **86**, 085408 (2012); J. Klinovaja, P. Stano, and D. Loss, *Phys. Rev. Lett.* **109**, 236801 (2012); J. Klinovaja, P. Stano, A. Yazdani, and D. Loss, *Phys. Rev. Lett.* **111**, 186805 (2013).

³¹ J. Alicea, *Rep. Prog. Phys.* **75**, 076501 (2012).

³² T. D. Stanescu and S. Tewari, *J. Phys. Condens. Matter* **25**, 233201 (2013).

³³ S. B. Chung, H.-J. Zhang, X.-L. Qi, and S.-C. Zhang, *Phys. Rev. B* **84**, 060510 (2011).

³⁴ V. Shivamoggi, G. Refael, and J. E. Moore, *Phys. Rev. B* **82**, 041405(R) (2010).

³⁵ P. W. Brouwer, M. Duckheim, A. Romito, and F. von Oppen, *Phys. Rev. Lett.* **107**, 196804 (2011).

³⁶ Y. Niu, S. B. Chung, C.-H. Hsu, I. Mandal, S. Raghu, and S. Chakravarty, *Phys. Rev. B* **85**, 035110 (2012).

³⁷ I. Adagideli, M. Wimmer, and A. Teker, *Phys. Rev. B* **89**, 144506 (2014).

³⁸ J. D. Sau and S. Das Sarma, *Nat. Commun.* **3**, 964 (2012).

³⁹ A. R. Akhmerov, J. P. Dahlhaus, F. Hassler, M. Wimmer, and C. W. J. Beenakker, *Phys. Rev. Lett.* **106**, 057001 (2011).

⁴⁰ W. DeGottardi, D. Sen, and S. Vishveshwara, *New. J. Phys.* **13**, 065028 (2011).

⁴¹ W. DeGottardi, M. Thakurathi, S. Vishveshwara, and D. Sen, *Phys. Rev. B* **88**, 165111 (2013).

⁴² J. D. Sau, C. H. Lin, H.-Y. Hui, and S. Das Sarma, *Phys. Rev. Lett.* **108**, 067001 (2012).

⁴³ L.-J. Lang and S. Chen, *Phys. Rev. B* **86**, 205135 (2012).

⁴⁴ P. W. Brouwer, M. Duckheim, A. Romito, and F. von Oppen, *Phys. Rev. B* **84**, 144526 (2011).

⁴⁵ X. Cai, L.-J. Lang, S. Chen, and Y. Wang, *Phys. Rev. Lett.* **110**, 176403 (2013).

⁴⁶ V. Mourik, K. Zuo, S. M. Frolov, S. R. Plissard, E. P. A. M. Bakkers, and L. P. Kouwenhoven, *Science* **336**, 1003 (2012).

⁴⁷ M. T. Deng, C. L. Yu, G. Y. Huang, M. Larsson, P. Caroff, and H. Q. Xu, *Nano Lett.* **12**, 6414 (2012).

⁴⁸ L. P. Rokhinson, X. Liu, and J. K. Furdyna, *Nat. Phys.* **8**, 795 (2012).

⁴⁹ A. Das, Y. Ronen, Y. Most, Y. Oreg, M. Heiblum, and H. Shtrikman, *Nat. Phys.* **8**, 887 (2012).

⁵⁰ A. D. K. Finck, D. J. Van Harlingen, P. K. Mohseni, K. Jung, and X. Li, *Phys. Rev. Lett.* **110**, 126406 (2013).

⁵¹ O. Petrova, P. Mellado, and O. Tchernyshyov, *Phys. Rev. B* **88**, 140405(R) (2013).

⁵² T. Kitagawa, E. Berg, M. Rudner, and E. Demler, *Phys. Rev. B* **82**, 235114 (2010).

⁵³ N. H. Lindner, G. Refael, and V. Galitski, *Nat. Phys.* **7**, 490 (2011).

⁵⁴ L. Jiang, T. Kitagawa, J. Alicea, A. R. Akhmerov, D. Pekker, G. Refael, J. I. Cirac, E. Demler, M. D. Lukin,

and P. Zoller, Phys. Rev. Lett. **106**, 220402 (2011).

⁵⁵ Z. Gu, H. A. Fertig, D. P. Arovas, and A. Auerbach, Phys. Rev. Lett. **107**, 216601 (2011).

⁵⁶ T. Kitagawa, T. Oka, A. Brataas, L. Fu, and E. Demler, Phys. Rev. B **84**, 235108 (2011).

⁵⁷ N. H. Lindner, D. L. Bergman, G. Refael, and V. Galitski, Phys. Rev. B **87**, 235131 (2013).

⁵⁸ E. Suárez Morell and L. E. F. Foa Torres, Phys. Rev. B **86**, 125449 (2012).

⁵⁹ M. Trif and Y. Tserkovnyak, Phys. Rev. Lett. **109**, 257002 (2012).

⁶⁰ A. Russomanno, A. Silva, and G. E. Santoro, Phys. Rev. Lett. **109**, 257201 (2012).

⁶¹ V. M. Bastidas, C. Emery, G. Schaller, and T. Brandes, Phys. Rev. A **86**, 063627 (2012).

⁶² V. M. Bastidas, C. Emery, B. Regler, and T. Brandes, Phys. Rev. Lett. **108**, 043003 (2012).

⁶³ M. Tomka, A. Polkovnikov, and V. Gritsev, Phys. Rev. Lett. **108**, 080404 (2012).

⁶⁴ A. Gomez-Leon and G. Platero, Phys. Rev. B **86**, 115318 (2012), and Phys. Rev. Lett. **110**, 200403 (2013).

⁶⁵ B. Dóra, J. Cayssol, F. Simon, and R. Moessner, Phys. Rev. Lett. **108**, 056602 (2012).

⁶⁶ D. E. Liu, A. Levchenko, and H. U. Baranger, Phys. Rev. Lett. **111**, 047002 (2013).

⁶⁷ Q.-J. Tong, J.-H. An, J. Gong, H.-G. Luo, and C. H. Oh, Phys. Rev. B **87**, 201109(R) (2013).

⁶⁸ M. S. Rudner, N. H. Lindner, E. Berg, and M. Levin, Phys. Rev. X **3**, 031005 (2013).

⁶⁹ J. Cayssol, B. Dóra, F. Simon, and R. Moessner, Phys. Status Solidi RRL **7**, 101 (2013).

⁷⁰ Y. T. Katan and D. Podolsky, Phys. Rev. Lett. **110**, 016802 (2013).

⁷¹ A. Kundu and B. Seradjeh, Phys. Rev. Lett. **111**, 136402 (2013).

⁷² V. M. Bastidas, C. Emery, G. Schaller, A. Gómez-León, G. Platero, and T. Brandes, arXiv:1302.0781v2.

⁷³ T. L. Schmidt, A. Nunnenkamp, and C. Bruder, New J. Phys. **15**, 025043 (2013).

⁷⁴ A. A. Reynoso and D. Frustaglia, Phys. Rev. B **87**, 115420 (2013).

⁷⁵ C.-C. Wu, J. Sun, F.-J. Huang, Y.-D. Li, and W.-M. Liu, arXiv:1306.3870.

⁷⁶ P. M. Perez-Piskunow, G. Usaj, C. A. Balseiro, and L. E. F. Foa Torres, Phys. Rev. B **89**, 121401(R) (2014).

⁷⁷ M. Thakurathi, A. A. Patel, D. Sen, and A. Dutta, Phys. Rev. B **88**, 155133 (2013).

⁷⁸ M. Reichl and E. Mueller, arXiv:1404.3217.

⁷⁹ T. Kitagawa, M. A. Broome, A. Fedrizzi, M. S. Rudner, E. Berg, I. Kassal, A. Aspuru-Guzik, E. Demler, and A. G. White, Nat. Commun. **3**, 882 (2012); M. C. Rechtsman, J. M. Zeuner, Y. Plotnik, Y. Lumer, D. Podolsky, F. Dreisow, S. Nolte, M. Segev, and A. Szameit, Nature **496**, 196 (2013); M. C. Rechtsman, Y. Plotnik, J. M. Zeuner, D. Song, Z. Chen, A. Szameit, and M. Segev, Phys. Rev. Lett. **111**, 103901 (2013); G. Puentes, I. Gerhardt, F. Katschmann, C. Silberhorn, J. Wrachtrup, and M. Lewenstein, Phys. Rev. Lett. **112**, 120502 (2014).

⁸⁰ K. Nakada, M. Fujita, G. Dresselhaus, and M. S. Dresselhaus, Phys. Rev. B **54**, 17954 (1996).

⁸¹ M. Kohmoto and Y. Hasegawa, Phys. Rev. B **76**, 205402 (2007).

⁸² L. Cano-Cortés, C. Ortix, and J. van den Brink, Phys. Rev. Lett. **111**, 146801 (2013).

⁸³ C. Dutreix, M. Guigou, D. Chevallier, and C. Bena, arXiv:1309.1143v4.

⁸⁴ J. Klinovaja and D. Loss, Phys. Rev. X **3**, 011008 (2013).

⁸⁵ W. DeGottardi, M. Thakurathi, S. Vishveshwara, and D. Sen, Phys. Rev. B **88**, 165111 (2013).

⁸⁶ H.-J. Stöckmann, *Quantum Chaos* (Cambridge University Press, Cambridge, 1999).

⁸⁷ E. Lieb, T. Schultz, and D. Mattis, Ann. Phys. (NY) **16**, 407 (1961).

⁸⁸ K. Sengupta, I. Zutić, H.-J. Kwon, V. M. Yakovenko, and S. Das Sarma, Phys. Rev. B **63**, 144531 (2001).

⁸⁹ R. Rajaraman, arXiv:cond-mat/0103366.

⁹⁰ L.-M. Duan, E. Demler, and M. D. Lukin, Phys. Rev. Lett. **91**, 090402 (2003).

⁹¹ A. Micheli, G. K. Brennan, and P. Zoller, Nat. Phys. **2**, 341 (2006).

⁹² C. Zhang, V. W. Scarola, S. Tewari, and S. Das Sarma, Proc. Natl. Acad. Sci. USA **104**, 18415 (2007).

⁹³ Y.-J. Han, R. Raussendorf, and L.-M. Duan, Phys. Rev. Lett. **98**, 150404 (2007).